COBEM 2023 27TH INTERNATIONAL CONGRESS OF MECHANICAL ENGENEERING

ABCM Brazilian Society of Mechanical Sciences and Engineering
27th ABCM International Congress of Mechanical Engineering
December 04-08, 2023, Florianópolis-SC, Brazil

COB-2023-0751
A COMPARATIVE STUDY OF A TRANSITION MODEL WITH A FULL TURBULENCE MODEL ON THE AERODYNAMIC ANALYSIS OF A WIND TURBINE AIRFOIL

Anderson M. Ribeiro
Graduate Program in Computational Modeling, Federal University of Juiz de Fora. José Lourenço Kelmer St., São Pedro, Juiz de Fora, MG 36036-900, Brazil.
andersonmr254@gmail.com

Felipe S. Loureiro
Dept. of Thermal and Fluid Sciences, Federal University of São João del-Rei. Frei Orlando Sq., Center, São João del-Rei - MG, 36307-352, Brazil.
felipe.loureiro@ufsj.edu.br

Patrícia H. Hallak and Afonso C.C. Lemonge
Dept. of Applied and Computational Mechanics, School of Engineering, Federal University of Juiz de Fora. José Lourenço Kelmer St., São Pedro, Juiz de Fora, MG 36036-900, Brazil.
patricia.hallak@engenharia.ufjf.br, afonso.lemonge@ufjf.br

Abstract. *Wind energy is rapidly becoming an economically viable energy source as significant improvements in the performance of modern wind turbines are being achieved, which are also due to better understanding and CFD modelling of the flow field. Laminar boundary layers generate relatively low friction forces, whereas turbulent boundary layers result in relatively large friction forces, making the laminar flow more desirable over the body as much as possible, as a means of reducing drag. The lift is obtained only as long as the boundary layer can withstand the lift producing pressure gradients about the airfoil. However, the laminar boundary layer can withstand only negligible adverse pressure gradients without separation, which makes the transition to turbulent flow desired to occur before the major adverse gradients are encountered, otherwise it would be reached a definite laminar separation and stall, producing drag through both friction and pressure forces with loss of lift. On the transition, boundary layers then undergo a laminar separation and reattach as a turbulent boundary layer. The fully turbulent flow computation does not capture this phenomenon, which may significantly overpredict the friction drag. So it is of concern the transition to turbulent boundary layer so, mainly, drag can be evaluated properly. A CFD analysis of an air flow with a* $Re = 3.0 \times 10^6$ *around the wind turbine airfoil NACA 63-215 was conducted under the finite volume method formulation in the OpenFOAM framework using a local correlation-based transition model (LCTM),* $\gamma - Re_\theta$*, based on two new transport equations, in addition to the* $SST\ k-\omega$ *equations; one for intermittency,* γ*, and another one for a transition onset criterion,* Re_θ*. The transport equations do not attempt to model the physics of the transition process itself, but implement transition correlations which account for transition due to freestream turbulence intensity, pressure gradients, and separation. Finally, the analysis was also carried out under the fully turbulent models Spalart-Allmaras and* $SST\ k-\omega$ *for comparison purposes with both the transition model results and experimental data. It was concluded that the fully turbulent model overpredicts the drag coefficient before the stall, mainly due to the friction drag, while the LCTM leads to a better drag coefficient curve when compared to the experimental data. This shows that accounting for the transition on the flow field modelling of this wind turbine airfoil has lead to better results.*

Keywords: *Laminar-turbulent transition, CFD, OpenFOAM, Wind turbine, airfoil*

1. INTRODUCTION

The fluid velocity and pressure around an airfoil are interconnected, contributing to lift (L) and drag (D) forces, as well as pitching moment (M). Lift and pitching moment arise from variations in velocity and pressure around the airfoil, while drag results from a combination of friction and pressure forces (Miley, 1982). The relative influence of friction and pressure on drag changes with the angle of attack, α, of the flow relative to the airfoil. Considering the relevant physical quantities, one can express these aerodynamic forces using standardized coefficients C_l for lift, C_d for drag and C_m for the pitching moment (Miley, 1982).

When a solid body moves relative to a fluid, a boundary layer forms around the body, characterized by significant viscous effects. Within the boundary layer, the flow exhibits complexity, with velocity transitioning from zero at the

body's surface to the value of the freestream flow outside the boundary layer. The flow in the boundary layer can exist in two states: laminar or turbulent. Laminar flow is smooth and uniform, resembling the freestream flow away from the body, while turbulent flow is characterized by an irregular and chaotic motion. Laminar flow destabilizes and changes to turbulent flow when certain physical limiting conditions within the boundary layer flow are exceeded. The process of this change is called transition (see Fig. 1a). Another important transition mechanism is separation-induced transition, where a laminar boundary layer separates due to a pressure gradient, leading to transition within the separated shear layer, which may or may not reattach (Malkiel and Mayle, 1996).

The magnitude of the friction force depends on the type of boundary layer and the Reynolds number. Laminar boundary layers generate relatively low frictional forces, while turbulent boundary layers result in higher friction forces. Therefore, promoting laminar flow over the body's surface is desirable to reduce drag. Both laminar and turbulent boundary layers are influenced by the pressure gradient of the flow. An adverse pressure gradient, acting against the flow, eventually causes flow reversal near the body surface, moving towards the low-pressure region. In most cases, once flow reversal occurs in the boundary layer, the external flow pattern breaks down, resulting in flow separation (stall) from the body (see Fig. 1b). This leads to the formation of a large turbulent wake, potentially affecting either the upper or lower surface of the airfoil. Flow separation causes a decrease in lift and an increase in drag due to changes in flow pressure (Miley, 1982).

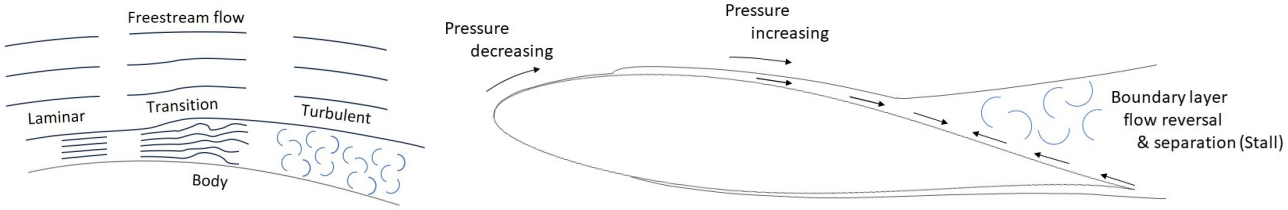

(a) (b)

Figure 1: Flow around the airfoil. a) Boundary layer flow adjacent to a solid body (airfoil) in a fluid flow. b) Boundary layer flow separation and subsequent stall.

The strength of adverse pressure gradients increases on the upper surface as the angle of attack rises, while it increases on the lower surface as the angle of attack decreases. The boundary layer responds to these adverse pressure gradients, leading to separation and stall. The laminar boundary layer is relatively weak and cannot withstand significant adverse pressure gradients. To prevent laminar separation and stall, transition to turbulent flow must occur before encountering major adverse gradients. Changes in lift and drag are attributed to increased boundary layer separation as the angle of attack increases or decreases (Miley, 1982). Factors such as Reynolds number, surface roughness, and turbulence intensity (TI) affect the boundary layer and consequently influence the lift and drag characteristics of the airfoil (Miley, 1982).

Another crucial transition mechanism occurs within the thin layer near the wall, known as the viscous sublayer, where viscous effects dominate (Cengel and Cimbala, 2013). The velocity profile within this layer is nearly linear, and the flow is streamlined. Due to the wall's presence, eddy motion is suppressed, resulting in an essentially laminar flow with shear stress dominated by laminar shear stress, which is proportional to fluid viscosity and the flow becomes turbulent as the normal distance to wall increases (Cengel and Cimbala, 2013).

The stability of the laminar boundary layer is affected by both the pressure gradient and Reynolds number, Re. Low Reynolds numbers and favorable pressure gradients increase stability. High Reynolds numbers and adverse pressure gradients reduce stability or destabilize. When subjected to an adverse pressure gradient, the laminar boundary layer may react in one of these ways: it may destabilize and become turbulent, it may separate and reattach shortly thereafter as a turbulent boundary layer, or it may separate and produce stall. The first behavior is depicted in Fig. 1a while the others are shown in Fig. 1b. It is important to mention that, this phenomenon is not captured by the fully turbulent models commonly used in computational fluid dynamics (CFD) analysis, which may directly affect the accuracy of the resultant aerodynamic forces (Miley, 1982).

It is of concern the transition to turbulent boundary layer so the aerodynamic forces can be evaluated properly. This paper presents a CFD analysis of a low turbulent ($TI = 0.3\%$) medium/high Reynolds air flow, $Re = 3.0 \times 10^6$, around the wind turbine airfoil NACA 63-215. The analysis was conducted under the finite volume method formulation in the OpenFOAM® framework using a local correlation-based transition model (LCTM) (Langtry and Menter, 2009), also known as $\gamma - Re_\theta$, based on two new transport equations, in addition to the well known $SST\, k-\omega$ model equations (Menter *et al.*, 2003); one for intermittency, γ, which can be used to trigger transition locally, and another one for a transition onset criterion, Re_θ, which captures the non-local influence of the turbulence intensity that changes due to the decay of the turbulence kinetic energy in the freestream, as well as due to changes in the freestream velocity outside the boundary layer. Finally, the analysis was also carried out under the fully turbulent models Spalart-Allmaras (Spalart and Allmaras, 1992) and $k - \omega\ SST$ (Menter *et al.*, 2003) for comparison purposes with both the transition model $\gamma - Re_\theta$ results and experimental data by Bertagnolio *et al.* (2001); Abbott and Albert (1959).

The present work is organized as follows. Section 2presents the statement of the problem by defining the computational domain, as well as the governing equations involved and the turbulence models used in the present work. The numerical experiments, the mesh and discretization schemes are discussed in Section 3., as well as the obtained results. Finally Section 4. highlights the main conclusions drawn from the studies performed.

2. GOVERNING EQUATIONS

For simplicity we confine our attention to incompressible flow, Newtonian fluid, constant-property and steady-state regime according to the Reynolds averaged Navier-Stokes (RANS) equations (Wilcox *et al.*, 1998)) and boundary conditions summarized below by Eq. (1). The governing equations are to be solved within the computational domain, Ω, which is enclosed by the boundary, $\partial\Omega = \Gamma_{inlet} \cup \Gamma_{outlet} \cup \Gamma_{wall}$, and defined in terms of the airfoil chord, c, as shown in Fig. 2.

$$\begin{cases} \frac{\partial(\rho U_j U_i)}{\partial x_j} = -\frac{\partial p}{\partial x_i} + \frac{\partial}{\partial x_j}\left(2\mu S_{ij} - \rho\overline{U_i' U_j'}\right) & \text{in } \Omega \\ \frac{\partial U_i}{\partial x_i} = 0 & \text{in } \Omega \\ U_i n_i < 0 \implies U_i = U_i^{\infty} \vee U_i n_i \geq 0 \implies \frac{\partial U_i}{\partial x_j} n_j = 0 & \text{on } \Gamma_{inlet} \\ U_i = 0 & \text{on } \Gamma_{wall} \\ \frac{\partial U_i}{\partial x_j} n_j = 0 & \text{on } \Gamma_{outlet} \end{cases} \tag{1}$$

where U_i and x_i are, respectively, velocity and position vectors, p is the pressure, ρ is the air density and U_i^{∞} the freestream velocity vector. The vector n_i is the unity vector normal to the boundary surface pointing outward the fluid domain. The term $2\mu S_{ij}$ is the viscous stress tensor, where μ is molecular viscosity and S_{ij} is the strain-rate tensor defined by $S_{ij} = \frac{1}{2}\left(\frac{\partial U_i}{\partial x_j} + \frac{\partial U_j}{\partial x_i}\right)$ (Wilcox *et al.*, 1998). The term $\rho\overline{U_i' U_j'}$ is the Reynolds-stress tensor, which is to be evaluated according to the turbulence models further explained.

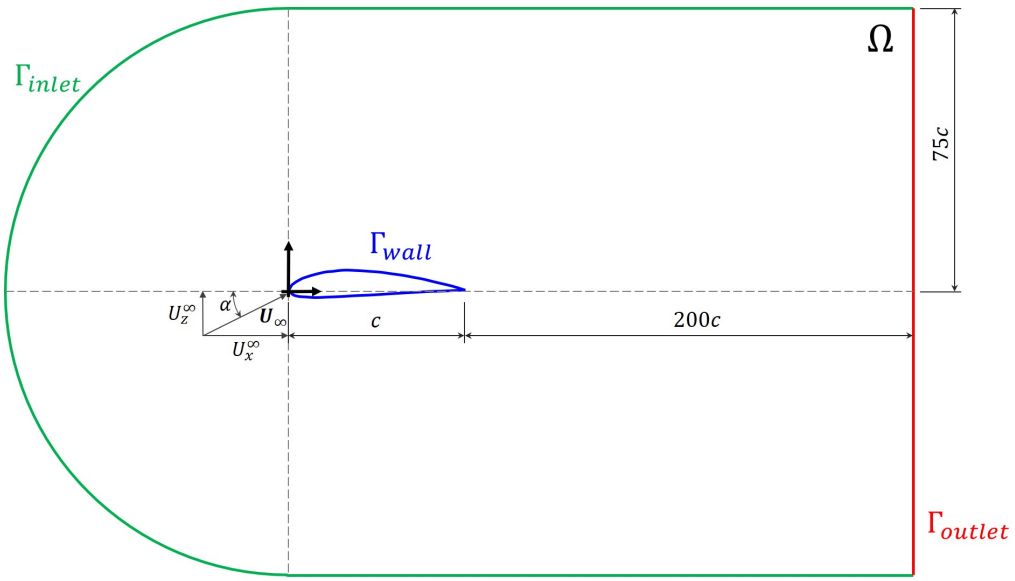

Figure 2: Fluid domain (not in scale) with each boundary label for boundary condition specification.

The Γ_{wall} boundary surface is defined according to the wind turbine airfoil NACA 63-215 section, obtained from Abbott and Albert (1959); Bertagnolio *et al.* (2001). In order to evaluate the aerodynamic coefficients along different angles of attack, α, the freestream wind speed, U_i^{∞}, components are defined accordingly, as: $U_x^{\infty} = U_{\infty}\cos(\alpha)$ and $U_z^{\infty} = U_{\infty}\sin(\alpha)$. For all cases, the Reynolds number, Re, in which the simulations were carried out is kept the same as well as the turbulent intensity, TI. The inlet freestream wind velocity is set up as Dirichlet boundary at the farfied boundaries assuming U_i^{∞}. Otherwise, according to the volume flux direction (inward or outward of the domain), the normal zero gradient Neumman boundary condition is applied. This is done mainly due to the form that the domain is posed, so for larger α values, the velocity might goes outward the domain even on Γ_{inlet} in the upper right corner of the domain.

2.1 TURBULENCE MODELS

The above Reynolds averaged equations are similar to the original conservation equations with the exception of the additional averaged products of the fluctuating components, $\rho\overline{U_i^{'}U_j^{'}}$. This introduces six new unknowns (the components of the Reynolds stress tensor) to the momentum equations (Lai *et al.*, 2009). Consequently the set of RANS equations is not closed and to be able to solve it additional equations for the unknown Reynolds stress components are required. The process of calculating these Reynolds stresses involves the use of turbulence models (Lai *et al.*, 2009).

The direct modeling of the Reynolds stress tensor is based on the Boussinesq hypothesis (Boussinesq, 1877), which in analogy with Newtonian flows assumes the Reynolds stress to be a linear function of the mean velocity gradients such that: $-\rho\overline{U_i^{'}U_j^{'}} = 2\mu_T S_{ij} - \frac{2}{3}\rho k\delta_{ij}$, with δ_{ij} being the Kronecker delta, k the turbulent kinetic energy and μ_T the turbulent viscosity. This still demands the knowledge of such fields as k and μ_T. Several turbulence models based on the Boussinesq hypothesis have been developed to address this issue (Wilcox *et al.*, 1998).

The two equations $k-\omega\ SST$ turbulence model, proposed by Menter *et al.* (2003), resolves additional transport equations for the turbulence kinetic energy, k, and turbulence specific dissipation rate, ω. It evaluates μ_T as: $\mu_T = \frac{a_1 k}{\max(a_1\omega, SF_2)}$, where S is the invariant measure of the strain rate, F_2 is a blending function and a_1 is one of the model's constants (see Menter *et al.* (2003) for more details). Suitable for complex boundary layer flows under adverse pressure gradient and separation (external aerodynamics and turbo-machinery), it provides accurate prediction of flow separation (Menter *et al.*, 2003). However, the $k-\omega\ SST$ is a fully turbulent model, which does not account for flow transition from laminar to turbulent.

In order to capture the transition effects on the simulations, it is applied the local correlation-based transition model (LCTM) (Langtry and Menter, 2009), also known as $\gamma - Re_\theta$, based on two new transport equations, in addition to the $SST\ k-\omega$ equations, as shown in Eq. (2); i.e., one equation is for intermittency, γ, which is coupled with the $SST\ k-\omega$ model to turn on the production term of the turbulent kinetic energy downstream of the transition point, based on the relation between transition momentum-thickness and strain-rate Reynolds number (Langtry and Menter, 2009). The other equation aims the transition onset criterion, $\hat{Re}_{\theta t}$, which captures the non-local influence of the turbulence intensity, which changes due to the decay of the turbulence kinetic energy in the freestream, as well as due to changes in the freestream velocity outside the boundary layer. This second transport equation is an essential part of the model as it ties the empirical correlation to the onset criteria in the intermittency equation.

$$
\begin{cases}
\frac{\partial(\rho U_i k)}{\partial x_i} = \hat{P}_k - \hat{D}_k + \frac{\partial}{\partial x_i}\left[(\mu + \sigma_k\mu_T)\frac{\partial k}{\partial x_i}\right] & \text{in } \Omega \\
\frac{\partial(\rho U_i \omega)}{\partial x_i} = P_\omega - D_\omega + \frac{\partial}{\partial x_i}\left[(\mu + \sigma_\omega\mu_T)\frac{\partial \omega}{\partial x_i}\right] + 2(1-F_1)\frac{\rho\sigma_{\omega 2}}{\omega}\frac{\partial k}{\partial x_i}\frac{\partial \omega}{\partial x_i} & \text{in } \Omega \\
\frac{\partial(\rho U_i \gamma)}{\partial x_i} = \hat{P}_\gamma - \hat{E}_\gamma + \frac{\partial}{\partial x_i}\left[(\mu + \frac{\mu_T}{\sigma_f})\frac{\partial \gamma}{\partial x_i}\right] & \text{in } \Omega \\
\frac{\partial\left(\rho U_i \hat{Re}_{\theta t}\right)}{\partial x_i} = \hat{P}_{\theta t} + \frac{\partial}{\partial x_i}\left[\sigma_{\theta t}(\mu + \mu_T)\frac{\partial \hat{Re}_{\theta t}}{\partial x_i}\right] & \text{in } \Omega \\
U_i n_i < 0 \implies k = \frac{0.1\mu U_\infty}{\rho L} \vee U_i n_i \geq 0 \implies \frac{\partial k}{\partial x_j} n_j = 0 & \text{on } \Gamma_{inlet} \cup \Gamma_{outlet} \\
k = 0 & \text{on } \Gamma_{wall} \\
U_i n_i < 0 \implies \omega = \frac{10 U_\infty}{L} \vee U_i n_i \geq 0 \implies \frac{\partial \omega}{\partial x_j} n_j = 0 & \text{on } \Gamma_{inlet} \cup \Gamma_{outlet} \\
\omega = 10\frac{6\nu}{\beta_1(\Delta d_1)^2} & \text{on } \Gamma_{wall} \\
U_i n_i < 0 \implies \gamma = 1.0 \vee U_i n_i \geq 0 \implies \frac{\partial \gamma}{\partial x_j} n_j = 0 & \text{on } \Gamma_{inlet} \cup \Gamma_{outlet} \\
\frac{\partial \gamma}{\partial x_j} n_j = 0 & \text{on } \Gamma_{wall} \\
U_i n_i < 0 \implies \hat{Re}_{\theta t} = \hat{Re}_{\theta t_\infty} \vee U_i n_i \geq 0 \implies \frac{\partial \hat{Re}_{\theta t}}{\partial x_j} n_j = 0 & \text{on } \Gamma_{inlet} \cup \Gamma_{outlet} \\
\frac{\partial \hat{Re}_{\theta t}}{\partial x_j} n_j = 0 & \text{on } \Gamma_{wall}
\end{cases}
\tag{2}
$$

The farfield boundary conditions values are defined according to NASA (2023), COMSOL Multiphysics® (COMSOL, 2022), Greenshields and Weller (2022) and Langtry and Menter (2009), which also provided the empirical relations for defining $\hat{Re}_{\theta t_\infty}$ as a function of TI. In addition, $L = 200c$ is the wake domain characteristic length, β_1 is one of SST model constants and Δd_1 the first cell center normal distance to the wall. The transition model interacts with the SST turbulence model (Menter *et al.*, 2003) through the $\hat{P}_k$ and $\hat{D}_k$ terms, where $\hat{P}_k = \gamma_{eff} P_k$ and $\hat{D}_k = \min(\max(\gamma_{eff}, 0.1), 1.0) D_k$. P_k and D_k are the original production and destruction terms for the SST model with σ_f being one of the constants for the intermittency and γ_{eff} a function of γ defined in Langtry and Menter (2009) work. For more details on the models coupling, the reader is referred to Langtry and Menter (2009). It is important to consider that, in order to capture the laminar and transitional boundary layers correctly, the grid must have the non-dimensional parameter $y^+ \approx 1$ at the first grid point off the wall (Langtry and Menter, 2009). The non-dimensional parameter y^+ is calculated according to the normal distance of the first cell center to the wall (Wilcox *et al.*, 1998). If the y^+ is too large (i.e., $y^+ > 5$), then the transition onset location moves upstream with increasing y^+. It should be noted that the

ω transport equation is kept the same of Menter *et al.* (2003) in the LCTM, where P_ω and D_ω are the production and destruction terms, σ_ω and $\sigma_{\omega 2}$ are some of the model constants and F_1 a blending function.

The transport equation for the intermittency γ accounts for transition source, $\hat{P}_\gamma$, which is defined according to strain-rate magnitude, empirical correlations that control the length of the transition region and transition onset location. The destruction/relaminarization term, $\hat{E}_\gamma$, is defined considering the vorticity magnitude and acts like a sink on the γ transport equation (Langtry and Menter, 2009). The term σ_f is one of the LCTM constants. The boundary condition for γ at the wall is zero normal flux, while for the farfield boundaries γ is equal to 1.0, where the volume flux goes inward the fluid domain, and assumes zero normal gradient case whether the normal volume flux goes outward of the domain. An inlet γ equals to 1.0 is necessary to preserve the original turbulence model's freestream turbulence decay rate (Langtry and Menter, 2009).

The transport equation for the transition momentum-thickness Reynolds number $\hat{Re}_{\theta t}$ uses a source term $P_{\theta t}$, which is designed to force the transported scalar $\hat{Re}_{\theta t}$ to match the local value of $Re_{\theta t}$ calculated from the empirical correlation. The boundary condition for $\hat{Re}_{\theta t}$ at the wall is zero flux. The boundary condition for $\hat{Re}_{\theta t_\infty}$ at the inlet should be calculated from the empirical correlation available in the original paper (Langtry and Menter, 2009) based on the inlet turbulence intensity.

Along the wall defined by Γ_{wall}, the OpenFOAM wall function **kLowReWallFunction** provides a turbulence kinetic energy imposed condition for low and high Reynolds formulation turbulent flow cases, i.e., in case the first cell non-dimensional distance, y^+, lies in either viscous sublayer or inertial layer (Liu, 2016). After getting y^+ value, it comes to the calculation of k^+ according to the following wall function definition (see Liu (2016); Kalitzin *et al.* (2005) and OpenFOAM documentations for further details):

$$k^+ = \begin{cases} \frac{C_k}{\kappa} \times \log(y^+) + B_k & \text{if } y^+ \geq 11.5 \\ \frac{2400}{C_{eps2}^2} \times C_f & \text{if } y^+ < 11.5 \end{cases} \tag{3}$$

where C_f is the friction coefficient, κ the von karma constant and the parameters C_k and C_{eps2} are defined in Liu (2016) work. The final k is obtained through k^+ and the friction velocity, as: $k = k^+ \times u_\tau^2$.

The OpenFOAM ω wall function, **omegaWallFunction**, given below, provides the constraint on turbulence specific dissipation. The ω wall function provides the combination of viscous and log equation according to the position of y^+ (Liu, 2016). In the intersection of the viscous sublayer and log-law region value is calculated through blending the viscous and log-law sublayer value.

$$\omega = \begin{cases} \omega_{Vis} = \frac{6.0\nu}{\beta_1 y^2} & \text{if } y^+ \leq 5 \\ \omega_{Log} = \frac{k^{1/2}}{C_\mu^{1/4} \kappa y} & \text{if } 30 \leq y^+ \leq 200 \\ \sqrt{\omega_{Vis}^2 + \omega_{Log}^2} & \text{if } 5 < y^+ < 30, \end{cases} \tag{4}$$

where C_μ is one of $SST\ k-\omega$ constants. As purpose of comparison, the simulations were also conducted under the fully turbulent models $SST\ k-\omega$ (Menter *et al.*, 2003) and Spalart-Allmaras (Spalart and Allmaras, 1992). It should be noted that for the $SST\ k-\omega$, the transport equations were solved as stated by Menter *et al.* (2003) and the boundary conditions used for k and ω are shown in Eq.(2). The Spalart-Allmaras implies solving just one additional transport equation, in contrast to the four equation model presented in Eq. (2), for a modified turbulent viscosity $\hat{\nu}$, which behaves linearly near the wall, not being necessary the usage of wall functions, but $y^+ \approx 1.0$. This is a one equation model, suitable for external aerodynamics, turbo-machinery and high speed flows, and reasonably accurate for mildly complex external/internal flows and boundary layer flows under pressure gradient (e.g., airfoils, wings, airplane fuselages, ship hulls) (Spalart and Allmaras, 1992).

3. NUMERICAL EXPERIMENTS

As defined in Section 2, the simulations were conducted under different freestream wind velocity vector, U_i^∞, according to each angle of attack, α, which assumes the following values for each case: $\alpha = \{0°, 5°, 8°, 10°, 12°, 13°, 15°, 17°\}$. It is noted that for all the cases the same medium/high Reynolds number, $Re = \frac{U_\infty \times c}{\nu} = 3.0 \times 10^6$, is set up, which accounts for the airfoil chord of $c = 1$ m, the freestream wind speed magnitude of $U_\infty = 1$ m/s and, in order to yield the established Re value, the air kinematic viscosity assumes the value of $\nu = 3.3333 \times 10^{-7}$ m^2/s, which implies $\rho = 1$ kg/m^3. The same holds for all the three used turbulence models for comparison of results.

The above defined Reynolds number is adopted due to the used experimental data for validation and verification of the simulations, which are taken from measurements performed at NASA low-turbulence pressure tunnel (Von Doenhoff and Abbott, 1947; Bertagnolio *et al.*, 2001), which takes $TI \approx 0.3\%$ for the given Re (Von Doenhoff and Abbott, 1947).

3.1 DISCRETIZATION AND NUMERICAL SCHEMES

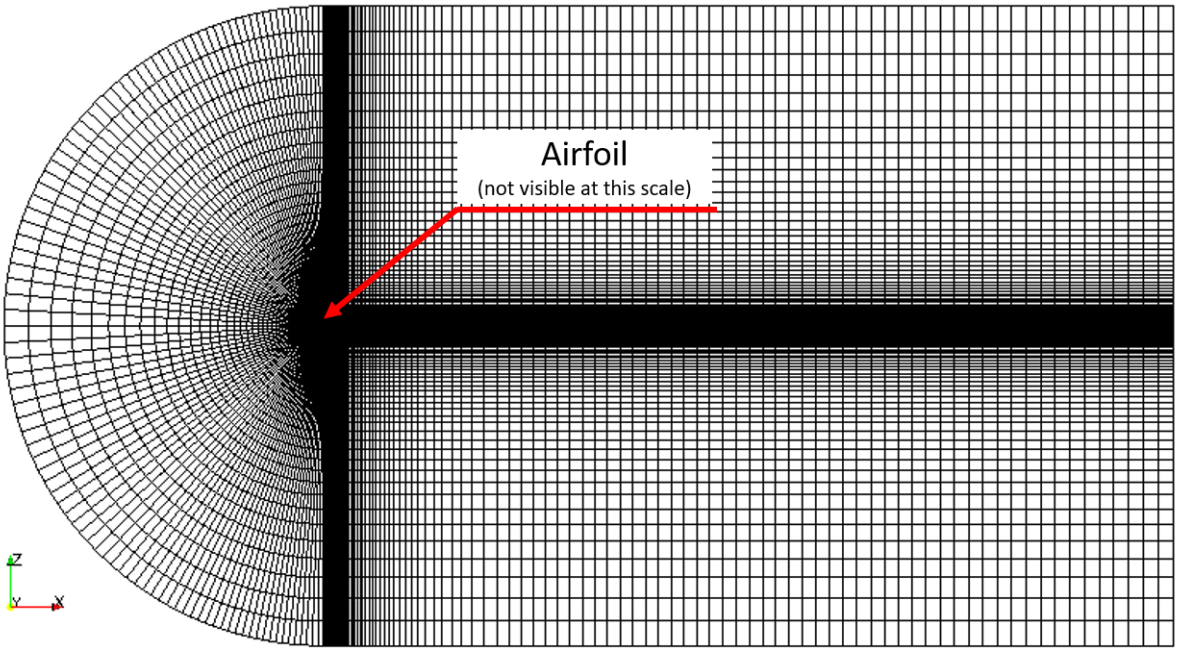

(a)

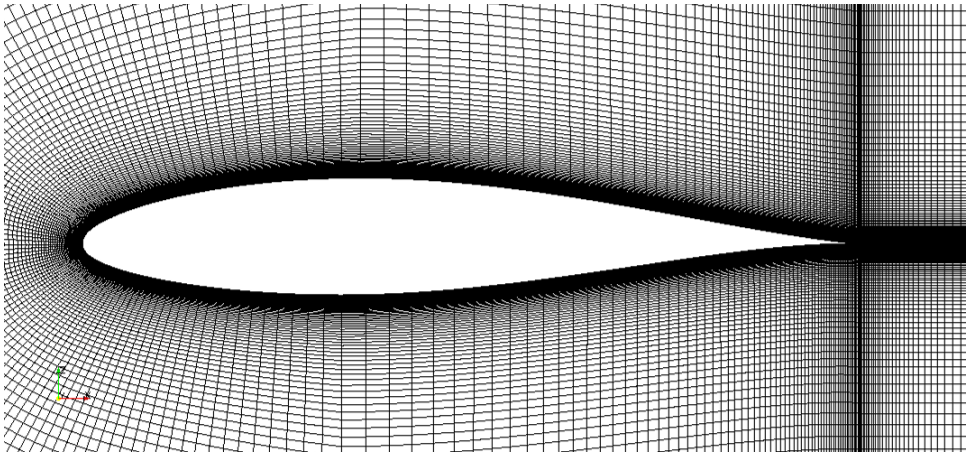

(b)

Figure 3: a) Mesh overview and b) zoom around the airfoil wall, Γ_{wall}, to show the mesh refinement.

The mesh was generated with the OpenFOAM grid generator (**blockMesh**), yielding a structured C-mesh configuration with 121,500 hexaedrical cells, as shown in Fig. 3, with the following mesh quality parameters: Mesh non-orthogonality Max. of 23.56474704°, average of 5.065592984° and Max. skewness of 0.3977354682. The average height of the cell at the airfoil was $y \approx 8.727587117621465 \times 10^{-6}$m. The mesh used for the NACA 63-215 airfoil, and details of regions of interest, are displayed in Fig. 3. As it can be seen, the mesh lines were extended in the wake of the trailing edge in order to stabilize the computations and do not compromise results accuracy.

The far field boundaries are also very far away (75 to 200 times the airfoil chord), to minimize issues associated with the effect of the farfield boundary (which can particularly influence drag and lift levels at high lift conditions) (NASA, 2023; Cengel and Cimbala, 2013). The mesh is very fine near the airfoil to resolve the boundary layer.

The used discretization schemes were Gauss with limiters on the gradient terms; second order upwind on momentum equations for the convective term and TVD (Total Variation Diminishing) schemes for scalar transport equations (turbulent quantities transport equations). The Gauss linear with non-orthogonality correction steps was used for the diffusion terms due to the low Max. non-orthogonality.

The pressure–velocity coupling can be resolved by adopting an iterative solution strategy such as the SIMPLE (Semi-Implicit Method for Pressure Linked Equations) algorithm (Caretto *et al.*, 1973) and SIMPLEC (Semi-Implicit Method for Pressure Linked Equations-Consistent) algorithm (Van Doormaal and Raithby, 1984). The SIMPLE algorithm was used for the Spalart-Allmaras turbulence model simulations while SIMPLEC for both $k - \omega\, SST$ and $\gamma - Re_\theta$ models. Both pressure-velocity coupling algorithms are implemented in OpenFOAM through **simpleFOAM** application.

As the solution to the discretized system of equations defined by Eq. (1) and Eq. (2) is sought, the error in the balance equation is quantified by defining residual error as Darwish and Moukalled (2016), according to the discretized equation. It is clear that when the solution is reached and the equation satisfied, the value of the residual will be zero or under a vanishing quantity ϵ. In OpenFOAM, the convergence of the solution is reached when the maximum value of the scaled absolute residuals has dropped below ϵ (see OpenFOAM documentation for further details). It was required for the scaled residuals to be of the order of $\epsilon \leq 10^{-5}$ for pressure equation in both pressure-velocity coupling algorithms and $\epsilon \leq 10^{-6}$ for all the other field equations so the solution is accepted as converged. The aerodynamic coefficients were verified as convergence monitors along side the residuals through iterations which have reached the ergodic and stationary regime.

3.2 RESULTS AND DISCUSSION

Numerical results were obtained for all the three used turbulence models discussed in Section 2. In this section, the obtained computational data are compared with measurements performed at NASA low-turbulence pressure tunnel (Abbott and Albert, 1959; Bertagnolio *et al.*, 2001) as well as with computational results from literature by Bertagnolio *et al.* (2001), which performed numerical simulations using the $k-\omega SST$ turbulence model coupled with transition model by Michel (1951) together with the empirical function given by Chen and Thyson (1971) for modelling the turbulence intermittency in their in-house developed code, *EllipSys2D - DTU*. Results are presented in Fig. 4 as lift, drag and pitching moment coefficients as function of angle of attack α.

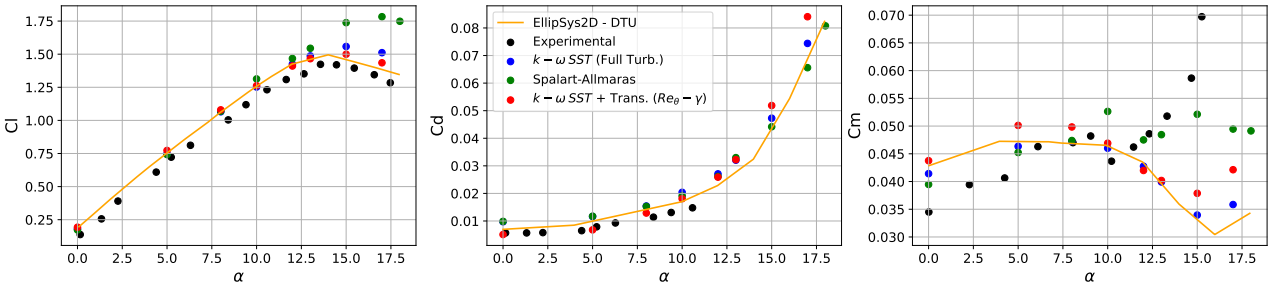

Figure 4: NACA 63-215 aerodynamic coefficients. (left) lift coefficient; (middle) drag coefficient and (right) pitching momentum coefficient.

It can be seen that the Spalart Allmaras turbulence model gives satisfactory results in attached boundary layer with favorable and minors adverse pressure gradients. However, it performs poorly with large adverse gradient and flow with strong separation, i.e., for large α values, mainly for C_l, where the skin-friction term loses its influence in the momentum equation. This is a model drawback, as also reported in the original paper of Spalart and Allmaras (1992) where they pointed out this limitation to deal with massive flow separation.

Conversely, the SST model successfully captured flow separation for larger alpha values, as mentioned by Menter *et al.* (2003) in their research. They claimed that the model accurately predicts aeronautics flows with strong adverse pressure gradients and separation. However, the model slightly overpredicts the lift coefficient (C_l) after stall (large α values) and the drag coefficient (C_d) for small α values. This discrepancy may be attributed to the assumption of fully turbulent flow of the model, which leads to a larger contribution of friction drag compared to laminar friction drag. This effect becomes more pronounced in low turbulence intensity flow regimes, such as the one simulated using low turbulent wind tunnel measurements for validation. The Spalart-Allmaras turbulence model also yielded similar C_d values for small α values. On the other hand, the $\gamma - Re_\theta$ transition turbulence model exhibits improved performance in predicting both the lift coefficient (C_l) and drag coefficient (C_d) across these two α value regions. Regarding the pitching momentum coefficient, it is noteworthy that both the $\gamma - Re_\theta$ and $k - \omega\, SST$ turbulence models have yielded similar results when compared with results from *EllipSys2D - DTU* (Bertagnolio *et al.*, 2001).

Specifically, the $k - \omega\, SST$ turbulence model has been shown to overestimate lift coefficients beyond the stall points, as highlighted by Chitsomboon and Thamthæ (2011). This overprediction is believed to stem from higher turbulence levels (and hence turbulent eddy viscosities) in the boundary layers due to the assumption of fully turbulent flow, which neglects the presence of a transition region. Consequently, momentum transfers to the near-wall regions are enhanced, allowing the boundary layer to more easily withstand adverse pressure gradients and increase lift after stall. The neglect of transition regions upstream by the fully-developed turbulence model further exacerbates this effect, as the boundary layer retains more energy due to higher eddy viscosities (and momentum transfers) resulting from the assumption of

full turbulence (Chitsomboon and Thamthæ, 2011). This discrepancy arises from the delayed separation of the turbulent boundary layer under adverse pressure gradient conditions on the suction side of the airfoil (Matyushenko and Garbaruk, 2016). Additionally, the elimination of the laminar-turbulent transition effect is suggested as one possible reason, as mentioned by Wieghardt and Tillmann (1951), and it is accounted by the $\gamma - Re_\theta$, which may explain the better results across these two α regions, as above mentioned.

As discussed and illustrated in Fig. 4, the $\gamma - Re_\theta$ model yielded superior performance. Consequently, a mesh sensitivity analysis was conducted based on the results obtained with this turbulence model, as detailed in Tab. 1, considering three levels of mesh refinement. The analysis aimed to assess the differences in results for two values of α in comparison to the utilized mesh (Mesh 2) of Fig. 3. For the lift coefficient (C_l), the differences were 0.45% for $\alpha = 5°$ and 4.31% for $\alpha = 17°$, when compared to Mesh 2. In the case of the drag coefficient (C_d), there was a difference of 1.44% between Meshes 2 and 3 for $\alpha = 5°$, whereas the difference was 11.67% between Meshes 1 and 2 for C_d. For $\alpha = 17°$, the difference was 8.1% when comparing Meshes 2 and 3. Finally, differences in terms of the pitching moment coefficient (C_m) were 0.7% for $\alpha = 5°$ and 7.73% for $\alpha = 17°$.

Table 1: Grid sensitivity analysis.

Mesh refinement	$\mathbf{C_l}$		$\mathbf{C_d}$		$\mathbf{C_m}$	
	$\alpha = \mathbf{5°}$	$\alpha = \mathbf{17°}$	$\alpha = \mathbf{5°}$	$\alpha = \mathbf{17°}$	$\alpha = \mathbf{5°}$	$\alpha = \mathbf{17°}$
Mesh 1 - 30,510 cells	0.769787	1.496879	0.007579	0.076891	0.049765	0.038996
Mesh 2 - 121,500 cells (utilized mesh)	0.772911	1.434943	0.006784	0.084075	0.050121	0.042126
Mesh 3 - 272,970 cells	0.774230	1.485150	0.006689	0.077269	0.050271	0.038867

Figure 5 shows the distribution of the pressure coefficient (C_p) along the airfoil's chord for two values of α, obtained using the $\gamma - Re_\theta$ model with Mesh 2. We compare these results to those reported by Bertagnolio *et al.* (2001) since experimental data for the specific airfoil and Reynolds number (Re) in question were not available (to the best of the author's knowledge). The comparison presented in Fig. 5 indicates a favorable agreement between the obtained results and the literature data. Finally, Fig. 6 shows the velocity magnitude, pressure and turbulent viscosity fields around the airfoil for the $\alpha = 15°$ case, obtained with the $\gamma - Re_\theta$ turbulence model.

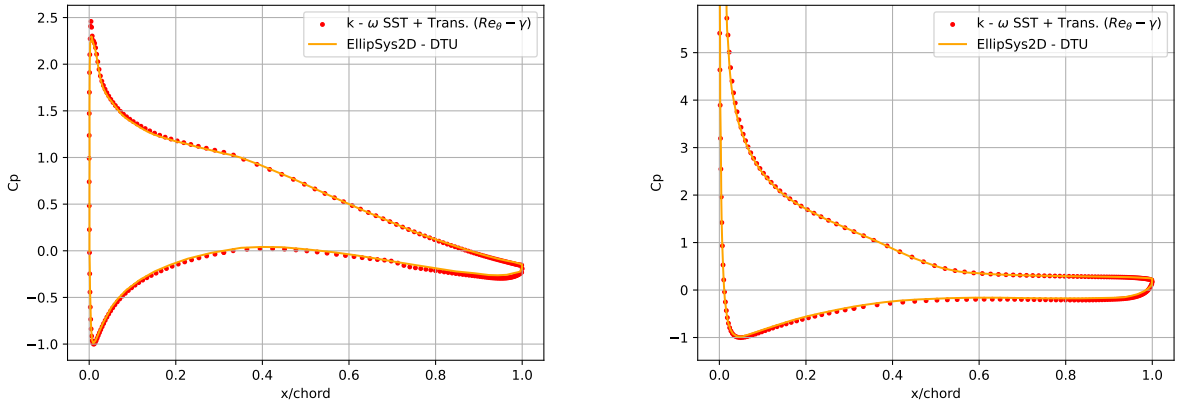

(a) $\alpha = 6°$ (b) $\alpha = 16°$

Figure 5: Pressure coefficient distribution along chord for a) $\alpha = 6°$ and b) $\alpha = 16°$ in comparison with data from Bertagnolio *et al.* (2001).

4. CONCLUSION

It can be pointed out that the utilization of the $\gamma - Re_\theta$ transition turbulence model in this aerodynamic analysis of the NACA 63-215 wind turbine airfoil with $Re = 3.0 \times 10^6$ and $TI = 0.3\%$ provides several significant contributions. Firstly, it addresses the limitations of fully turbulent flow assumptions, in which the $k - \omega\, SST$ and Spalart-Allmaras turbulence models rely, by considering the presence of transition regions in the boundary layer. This consideration provides a more accurate representation of the flow behavior, particularly in scenarios involving adverse pressure gradients and flow separation, leading to better lift coefficient (C_l) and drag coefficient (C_d) results. It helps overcome the overprediction issues observed in fully turbulent models beyond the stall points, resulting in better agreement between simulations and experimental data.

The inclusion of the transition turbulence model in airfoil analysis reveals the importance of laminar-turbulent transition phenomena and their impact on aerodynamic characteristics. This consideration results in a more comprehensive

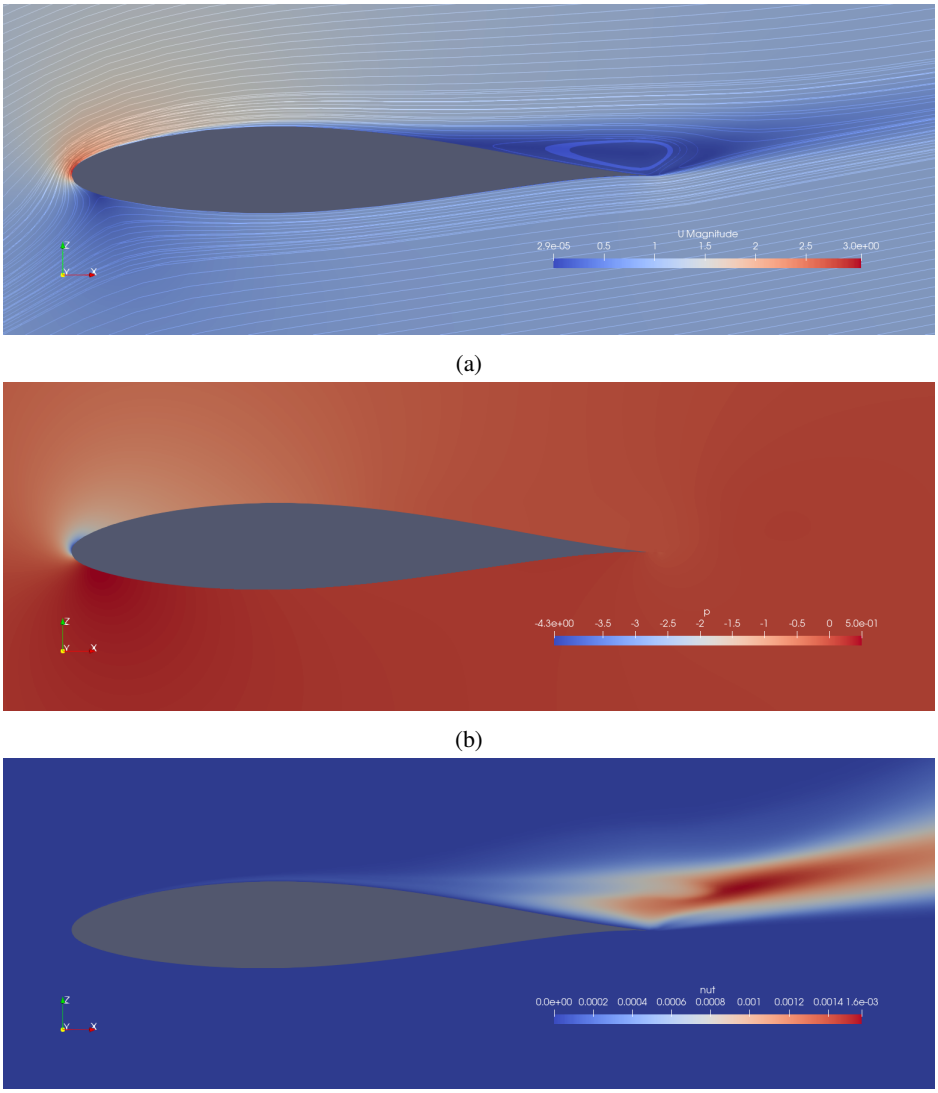

(a)

(b)

(c)

Figure 6: a) velocity magnitude, b) pressure p, and c) turbulent viscosity μ_T result fields for the $\alpha = 15^\circ$ case with the $\gamma - Re_\theta$ model.

understanding of the flow behavior, particularly in low turbulence intensity regimes, as verified here for the analyzed case in which the simulation results were compared to the measurements performed at NASA low-turbulence pressure tunnel.

5. ACKNOWLEDGEMENTS

The authors thank the Graduate Program in Computational Modeling (PPGMC/UFJF), Federal University of Juiz de Fora (UFJF), Federal University of São João del-Rei (UFSJ). The authors also wish to thank to CAPES (Finance Code 001), CNPq (Grants 308105/2021-4 and 303221/2022-4), and FAPEMIG (Grants TEC PPM-00174-18 and APQ-00869-22) for their support.

6. REFERENCES

Abbott, I.H. and Albert, E., 1959. "Von doenhoff. theory of wing sections".

Bertagnolio, F., Sørensen, N., Johansen, J. and Fuglsang, P., 2001. "Wind turbine airfoil catalogue".

Boussinesq, J., 1877. *Essai sur la théorie des eaux courantes*. Impr. nationale.

Caretto, L., Gosman, A., Patankar, S. and Spalding, D., 1973. "Two calculation procedures for steady, three-dimensional flows with recirculation". In *Proceedings of the Third International Conference on Numerical Methods in Fluid Mechanics: Vol. II Problems of Fluid Mechanics*. Springer, pp. 60–68.

Cengel, Y. and Cimbala, J., 2013. *Ebook: Fluid mechanics fundamentals and applications (si units)*. McGraw Hill.

Chen, K.K. and Thyson, N.A., 1971. "Extension of emmons' spot theory to flows on blunt bodies". *AIAA Journal*, Vol. 9,

No. 5, pp. 821–825.

Chitsomboon, T. and Thamthæ, C., 2011. "Adjustment of k-ω sst turbulence model for an improved prediction of stalls on wind turbine blades". In *World renewable energy congress*. pp. 4114–4120.

COMSOL, 2022. "COMSOL Multiphysics® v. 6.1". URL `https://www.comsol.com`.

Darwish, M. and Moukalled, F., 2016. *The finite volume method in computational fluid dynamics: an advanced introduction with OpenFOAM® and Matlab®*. Springer.

Greenshields, C. and Weller, H., 2022. *Notes on Computational Fluid Dynamics: General Principles*. CFD Direct Ltd, Reading, UK.

Kalitzin, G., Medic, G., Iaccarino, G. and Durbin, P., 2005. "Near-wall behavior of rans turbulence models and implications for wall functions". *Journal of Computational Physics*, Vol. 204, No. 1, pp. 265–291. ISSN 0021-9991. doi:https://doi.org/10.1016/j.jcp.2004.10.018. URL `https://www.sciencedirect.com/science/article/pii/S0021999104004164`.

Lai, W.M., Rubin, D. and Krempl, E., 2009. *Introduction to continuum mechanics*. Butterworth-Heinemann.

Langtry, R.B. and Menter, F.R., 2009. "Correlation-based transition modeling for unstructured parallelized computational fluid dynamics codes". *AIAA journal*, Vol. 47, No. 12, pp. 2894–2906.

Liu, F., 2016. "A thorough description of how wall functions are implemented in openfoam". *Proceedings of CFD with OpenSource Software*, Vol. 34.

Malkiel, E. and Mayle, R.E., 1996. "Transition in a Separation Bubble". *Journal of Turbomachinery*, Vol. 118, No. 4, pp. 752–759. ISSN 0889-504X. doi:10.1115/1.2840931. URL `https://doi.org/10.1115/1.2840931`.

Matyushenko, A.A. and Garbaruk, A.V., 2016. "Adjustment of the k-ω sst turbulence model for prediction of airfoil characteristics near stall". *Journal of Physics: Conference Series*, Vol. 769, No. 1, p. 012082. doi:10.1088/1742-6596/769/1/012082. URL `https://dx.doi.org/10.1088/1742-6596/769/1/012082`.

Menter, F.R., Kuntz, M. and Langtry, R., 2003. "Ten years of industrial experience with the sst turbulence model". *Turbulence, heat and mass transfer*, Vol. 4, No. 1, pp. 625–632.

Michel, R., 1951. "Etude de la transition sur les profiles d'aile; etablissement d'un critére de determination de point de transition et calcul de la trainee de profile incompressible". *ONERA Rep*, Vol. 1.

Miley, S.J., 1982. "Catalog of low-reynolds-number airfoil data for wind-turbine applications". Technical report, Rockwell International Corp., Golden, CO (USA). Rocky Flats Plant; Texas A ....

NASA, C.R., 2023. "Turbulence modeling resource". https://turbmodels.larc.nasa.gov/. Accessed 02 Apr 2023.

Spalart, P. and Allmaras, S., 1992. "A one-equation turbulence model for aerodynamic flows". In *30th aerospace sciences meeting and exhibit*. p. 439.

Van Doormaal, J.P. and Raithby, G.D., 1984. "Enhancements of the simple method for predicting incompressible fluid flows". *Numerical heat transfer*, Vol. 7, No. 2, pp. 147–163.

Von Doenhoff, A.E. and Abbott, F.T., 1947. "The langley two-dimensional low-turbulence pressure tunnel". Technical report.

Wieghardt, K. and Tillmann, W., 1951. "On the turbulent friction layer for rising pressure". Technical report.

Wilcox, D.C. *et al.*, 1998. *Turbulence modeling for CFD*, Vol. 2. DCW industries La Canada, CA.

7. RESPONSIBILITY NOTICE

The authors are solely responsible for the printed material included in this paper.